

## Article

# Development of Hydrogen Fuel Cell–Battery Hybrid Multicopter System Thermal Management and Power Management System Based on AMESim

JiHyun Choi <sup>1</sup>, Hyun-Jong Park <sup>1,2,3,\*</sup>  and Jaeyoung Han <sup>1,2,3,\*</sup>

<sup>1</sup> Department of Future Automotive Engineering, Kongju National University, 1223-24 Cheonan-daero, Seobuk-gu, Cheonan-si 31080, Chungcheongnam-do, Republic of Korea; wlguswlgus04@smail.kongju.ac.kr

<sup>2</sup> Department of Mechanical Engineering, Kongju National University, 1223-24 Cheonan-daero, Seobuk-gu, Cheonan-si 31080, Chungcheongnam-do, Republic of Korea

<sup>3</sup> Institute of Green Car Technology, Kongju National University, 1223-24 Cheonan-daero, Seobuk-gu, Cheonan-si 31080, Chungcheongnam-do, Republic of Korea

\* Correspondence: phj@kongju.ac.kr (H.-J.P.); hjyt11@kongju.ac.kr (J.H.)

**Abstract:** Urban Air Mobility (UAM) is gaining attention as a solution to urban population growth and air pollution. Hydrogen fuel cells are applied to overcome the limitations of battery-based UAM, utilizing a PEMFC (Polymer Electrolyte Membrane Fuel Cell) with batteries in a hybrid system to enhance responsiveness. Power management improves efficiency through effective power distribution under varying loads, while thermal management maintains optimal stack temperatures to prevent degradation. This study developed a hydrogen fuel cell–battery hybrid multicopter system using AMESim, consisting of a 138 kW fuel cell stack, 60 kW battery, DC–DC converters, and thrust motors. A rule-based power management system was implemented to define power distribution strategies based on SOC and load demand. The system’s operating range was designed to allocate power according to battery SOC and load variations. For an initial SOC of 45%, the power management system distributed power for flight, and the results showed that the state machine control system reduced hydrogen consumption by 5.85% and parasitic energy by 1.63% compared to the rule-based system.



Academic Editor: Mario Marchesoni

Received: 18 December 2024

Revised: 13 January 2025

Accepted: 17 January 2025

Published: 20 January 2025

**Citation:** Choi, J.; Park, H.-J.; Han, J. Development of Hydrogen Fuel Cell–Battery Hybrid Multicopter System Thermal Management and Power Management System Based on AMESim. *Energies* **2025**, *18*, 447. <https://doi.org/10.3390/en18020447>

**Copyright:** © 2025 by the authors. Licensee MDPI, Basel, Switzerland. This article is an open access article distributed under the terms and conditions of the Creative Commons Attribution (CC BY) license (<https://creativecommons.org/licenses/by/4.0/>).

**Keywords:** Polymer Electrolyte Membrane Fuel Cell; UAM; Urban Air Mobility; PMS; power management system; TMS; thermal management system; hybrid system

## 1. Introduction

### 1.1. Research Background

The rapid increase in urban populations, traffic congestion, and air pollution have emerged as major challenges in modern society. In particular, the global issue of greenhouse gas emissions remains a critical task that must be urgently addressed to achieve sustainable development. As a new alternative to these problems, Urban Air Mobility (UAM) has been gaining attention. UAM offers the potential to alleviate urban traffic congestion and significantly reduce emissions from ground transportation, contributing to environmental pollution mitigation.

To realize this vision, eco-friendly technologies that enhance the efficiency and sustainability of UAM are essential. Current research on UAM systems is actively progressing, and among various UAM forms, multicopters typically use lithium-ion batteries as their primary power source. However, lithium-ion batteries face challenges due to their low energy density, making extended flight durations and high energy consumption during

operation difficult to address. Increasing the battery capacity to store more energy would result in increased weight, potentially degrading flight performance [1].

Hydrogen fuel cells, which emit no greenhouse gases and offer higher specific energy compared to batteries, are emerging as a promising alternative power source. In particular, Polymer Electrolyte Membrane Fuel Cells (PEMFCs), a type of fuel cell, are widely used for aircraft propulsion due to their low operating temperature, relatively high power density, and rapid response to load changes [2]. These characteristics make fuel cells a promising solution for enhancing UAM performance and improving flight efficiency.

## 1.2. Research Survey

Recent research on Urban Air Mobility (UAM) has been conducted by many researchers. Garrow et al. [3] presented future research directions for UAM expansion into air mobility based on data obtained from the EV and AV literature. Marzouk et al. [4] presented various models with different preparation stages, including differences and similarities between UAM and flying cars, commercially operating cases, and prototypes under development. Asmer et al. [5] estimated the global demand for UAM using a city-centric forecasting methodology for 990 cities and emphasized the need for UAM system optimization. Neto et al. [6] proposed the TUS (Trajectory-Based Urban Air Mobility Simulator) platform to evaluate the efficiency and safety of UAM, simulating various algorithms and trajectories. Ferrare et al. [7] evaluated the safety and performance of UAM scenarios where multiple UAVs share narrow airspace through multi-agent system (MAS) simulations. Research has also been conducted on UAM using a fuel cell–battery hybrid system. Apeland et al. [8] developed a fuel cell–battery hybrid system, which resulted in an increase of 43 min in flight time compared to battery-powered UAM. Corcou et al. [9] explored the feasibility of electric propulsion for training using a hybrid system with electric motors and fuel cells, evaluating the applicability of batteries and fuel cells. Marinaro et al. [10] conducted a study comparing the feasibility of switching from a battery-based configuration to a fuel cell-based configuration using Simcenter AMESim. An et al. [11] proposed and validated a sizing methodology to address the limited range and endurance issues of eVTOL UAVs by combining hydrogen fuel cells and batteries. Bing et al. [12] analyzed the degradation mechanisms of a three-cell PEMFC stack through 1600 h of durability testing, identifying voltage degradation, structural damage to the MEA, catalyst loss, and agglomeration as the primary causes. Milad et al. [13] proposed a fuel cell management system to control degradation factors such as high temperature, pressure fluctuations, and imbalance in fuel/oxidant supply in PEMFCs, and presented methods to extend the fuel cell's lifespan through modeling and experimental validation. Donateo et al. [14] reviewed the applicability of hydrogen fuel cells for UAV and UAM applications, studying the modeling and dynamic control of an air-cooled PEMFC system that adapts to varying operating conditions. Rafael et al. [15] assessed the design and feasibility of a hybrid hydrogen fuel powerplant for UAM rotorcraft and analyzed the impact of hybrid and fuel cell pressurization on efficiency and emissions reduction. Achour et al. [16] optimized the power of both fuel cells and batteries simultaneously through a particle swarm optimization algorithm, distributing the power according to the required power profile. Saib et al. [17] proposed a hybrid power management system (HPMS) combining frequency separation, power limitation, and fuzzy logic, validating the effectiveness and performance through laboratory testing after simulation in MATLAB/Simulink. Heran et al. [18] proposed a real-time parameter tuning method utilizing data-driven adaptive oxygen excess ratio control and a secondary active disturbance rejection controller. Lee et al. [19] demonstrated the utility of an active power management approach by applying a power management system that produced the required power through solar cells, fuel cells, and battery packs, maintaining a target charge state of 45% during a 3.8 h flight test. Erdör Türk et al. [20] extended the flight time of UAVs through

a hybrid power management system combining a 200 W PEM fuel cell and battery, showing that the fuel cell-based energy system could double the durability compared to a battery-only system. Zhou et al. [21] proposed an energy management strategy based on State Machine Control (SMC) for optimal power distribution between fuel cells and batteries, validating the system's dynamic performance through flight profile power demand. Additionally, Lee et al. [22] analyzed the impact of load fluctuations on fuel cell performance degradation and emphasized the importance of power management strategies to minimize this effect.

However, the aforementioned studies mainly focus on basic research on UAM and fuel cell–battery hybrid systems, and there is limited research on multicopter systems with fuel cell–battery hybrids using AMESim software 2310. Therefore, this study developed a multicopter system utilizing a fuel cell–battery hybrid system modeled with AMESim software. A comparative analysis was conducted by implementing and evaluating two power management systems: the Rule-Based power management system and the State Machine power management system. AMESim software integrates various physical domains, enabling precise analysis of complex system interactions. This allows for effective performance analysis based on the different domains of the system and provides essential information during the design optimization process. The developed UAM system model consists of a fuel cell system, including a fuel cell stack, hydrogen supply system, air supply system, and thermal management system, as well as a battery, converter, thrust motor, and their respective controllers. Additionally, a power management system that can appropriately distribute the load power between the fuel cell and battery is applied. As a result, the thermal management of the fuel cell and the system behavior of the fuel cell–battery hybrid multicopter under the power management system were analyzed.

## 2. System Configuration

The power supply system developed for the multicopter in this study adopts a hybrid system consisting of a fuel cell system and batteries, as illustrated in Figure 1. The fuel cell system comprises a fuel cell stack and Balance of Plant (BOP) components, enabling stable fuel supply and thermal management. The battery system includes three 20 kW battery packs, which serve as auxiliary power sources to ensure stable response during initial flight and rapid power surges in-flight. Additionally, the multicopter system incorporates converters for voltage transformation, efficiently converting the power generated by the fuel cell and batteries to meet the thrust motor's voltage requirements. The thrust motor is responsible for altitude control during flight through PI control, delivering output corresponding to the altitude and supporting stable flight. The fuel cell–battery system operates under a power management system to efficiently distribute output.

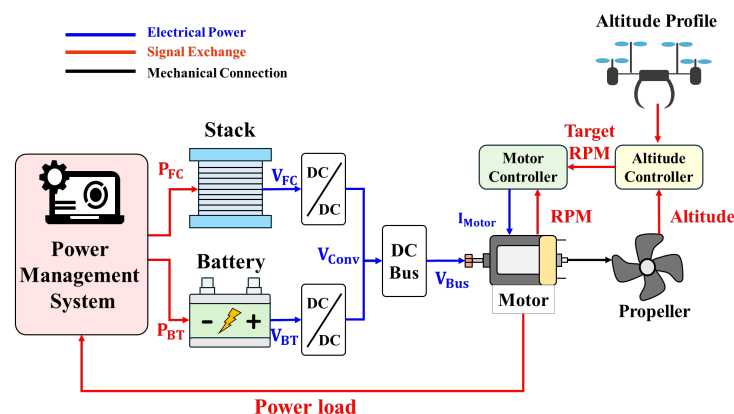


Figure 1. Fuel cell–battery hybrid multicopter system.

## 2.1. Fuel Cell System

### 2.1.1. Fuel Processing System

The operation of the fuel cell stack requires control at the required supply pressure, and thus a stable hydrogen supply system is essential. To maximize the high energy density and flight efficiency of UAM, most systems adopt hydrogen supply methods using high-pressure hydrogen tanks. Hydrogen is stored at pressures above 700 bar, and directly depressurizing it to supply to the fuel cell stack can lead to issues such as imprecise pressure control and system instability. Therefore, a two-stage depressurization system was applied, where the pressure is first reduced from 700 bar to 10 bar in the first stage, and then further reduced from 10 bar to 2.5 bar in the second stage, ensuring the hydrogen is supplied at the appropriate pressure [23].

### 2.1.2. Air Processing System

The air supply system plays a crucial role in reliably delivering oxygen essential for the electrochemical reaction in fuel cells. When applied to aircraft, variations in altitude result in changes in atmospheric pressure and density, creating challenges in maintaining a consistent air supply pressure. In particular, the 140 kW fuel cell system used in this study consumes significant power due to its large capacity but employs a pressurized compressor capable of supplying air at high pressure. The airflow equation for the air supply through the compressor is calculated as shown below, and the compressor data used in this study refer to the experimental data from [24].

$$\dot{m}_{air} = \frac{I \times O_{2, \text{stoi}} \times N_{cell}}{nF} \quad (1)$$

### 2.1.3. Stack

The fuel cell voltage equation is calculated using the Nernst equation ( $E_{Nernst}$ ), taking into account the activation loss voltage ( $V_{Act}$ ), ohmic loss voltage ( $V_{Ohm}$ ), and concentration loss voltage ( $V_{Con}$ ). The Nernst equation ( $E_{Nernst}$ ) is calculated as shown in Equation (2).

$$V_{Cell} = E_{Nernst} - V_{Act} - V_{Ohm} - V_{Con} \quad (2)$$

$$E_{Nernst} = -\frac{\Delta G_0^f}{nF} + \frac{RT}{nF} \ln \left( \frac{p_{H_2} (p_{O_2})^2}{p_{H_2O}} \right) \quad (3)$$

The activation loss voltage ( $V_{Act}$ ) is the internal loss voltage required to overcome the activation barrier of the electrochemical reaction, and it is represented by Equation (3). The ohmic loss voltage ( $V_{Ohm}$ ) arises from the intrinsic resistance to charge transport and is represented by Equation (4). The concentration loss voltage ( $V_{Con}$ ) occurs due to the concentration or mass transport of the reactant gases and is represented by Equation (5).

$$V_{Act} = \frac{RT}{\alpha nF} \log \left( \frac{j_{stack}}{j_0'} \right) \quad (4)$$

$$V_{Ohm} = R_{memb} I \quad (5)$$

$$V_{Con} = -B \log \left( 1 - \frac{j_{stack}}{j_l} \right) \quad (6)$$

The power and heat generated by the fuel cell stack are defined by Equations (6) and (7), respectively. The development was targeted for Ballard's FC-gen stack, and the specifications and performance curves of the fuel cell stack can be found in Table 1 and Figure 2.

$$P_{stack} = V_{cell} N_{cell} I \quad (7)$$

$$Q_{gen} = (E - V_{cell})N_{cell}I \quad (8)$$

**Table 1.** Fuel cell stack specifications.

System	Components	Parameters	Unit
Fuel Cell Stack	Number of cells	309	ea
	Active area	480	cm <sup>2</sup>
	Current	624	A
	Membrane thickness	0.0023	m
	Exchange current density	0.02	mA/cm <sup>2</sup>
	Limiting current density	1400	mA/cm <sup>2</sup>
	Mass	55	kg

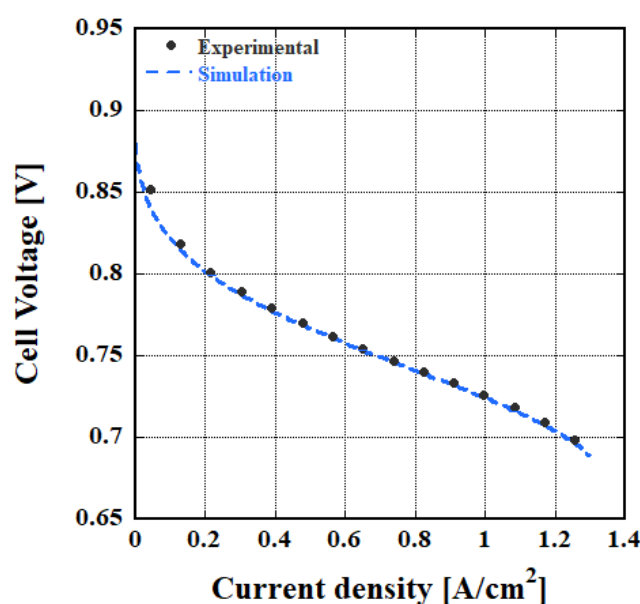


**Figure 2.** Polarization curve characteristic of fuel cell stack.

#### 2.1.4. Thermal Management System

The fuel cell stack operates most efficiently within a specific temperature range of 333.15 K to 353.15 K. If the stack temperature is too low, the electrochemical reaction rate decreases, resulting in reduced output. If the temperature is too high, the electrolyte may dry out, and thermal degradation of the components may occur. Therefore, it is essential to maintain an appropriate operating temperature [25–27]. In this study, a cooling system using coolant was applied to a high-capacity 138 kW fuel cell, as shown in Figure 3. The cooling system consists of a coolant pump to control the flow rate of the coolant, a three-way valve to increase the temperature of the stack from its initial low temperature to the operating temperature, a radiator, and a cooling fan to cool the high-temperature coolant after stack cooling through natural and forced convection. The coolant pump and cooling fan were developed based on a reference paper for a fuel cell system of the same capacity [28]. The developed coolant pump was controlled to 343.15 K based on the stack's exit temperature using a PI controller, and the cooling fan was controlled to 333.15 K based on the stack's inlet temperature using a PI controller. Additionally, the radiator facilitates heat exchange between the high-temperature coolant and the external environment, and it is calculated as follows.

$$\dot{Q} = \varepsilon \times \dot{Q}_{max} \quad (9)$$

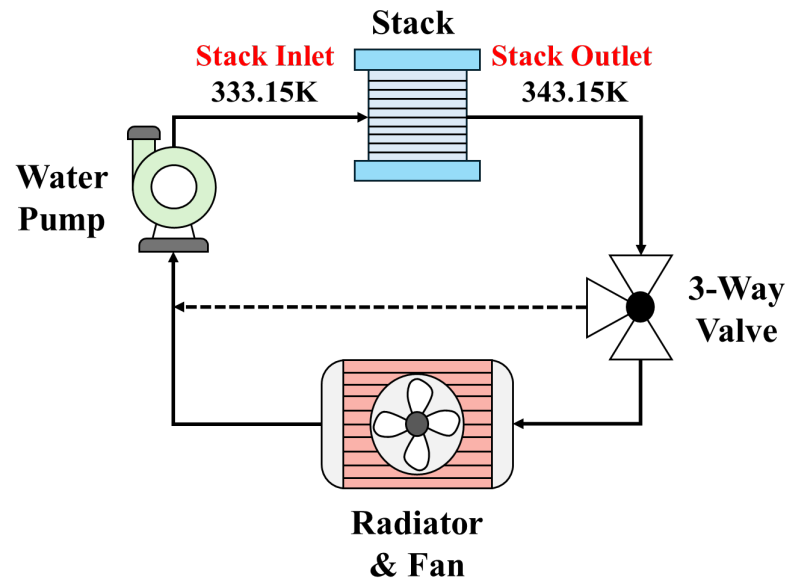


**Figure 3.** Fuel cell thermal management system structure.

Here,  $\dot{Q}$  represents the actual heat transfer rate,  $\varepsilon$  is the heat exchanger efficiency, and  $\dot{Q}_{max}$  is the maximum heat transfer rate of the heat exchanger. The maximum heat transfer rate is calculated based on the lower heat capacity  $c_{min}$  of the coolant and air, and the temperature difference between the coolant inlet temperature and the air inlet temperature, as shown below.

$$\dot{Q}_{max} = c_{min}(T_{coolant,in} - T_{air,in}) \quad (10)$$

Here,  $T_{coolant,in}$  represents the coolant inlet temperature at the radiator, and  $T_{air,in}$  represents the air inlet temperature at the radiator. The heat efficiency is calculated using the dimensionless number NTU (Number of Transfer Units) to evaluate the performance of the heat exchanger, as shown below.

$$\varepsilon = \frac{1 - \exp[-NTU(1 - c)]}{1 - c \times \exp[-NTU(1 - c)]} \quad (11)$$

Here,  $NTU$  is given by  $UA/C_{min}$ , which allows the evaluation of the heat exchanger's heat transfer performance. Using this, the heat efficiency can be calculated. Based on the calculated heat transfer rate, the coolant's radiator outlet temperature can be calculated as follows.

$$T_{coolant,out} = T_{coolant,in} - \frac{\dot{Q}}{c_{coolant}} \quad (12)$$

## 2.2. Battery

The battery is inevitably applied in a hybrid configuration with the fuel cell system to complement the slow reaction rate of the fuel cell and serve as an auxiliary power source to handle rapid load changes. The battery model was developed using the Simcenter AMESim Battery Pre-Sizing Tool, based on three criteria: target battery voltage, energy, and power. This Pre-Sizing Tool supports the initial design of the battery system and predicts the optimal battery capacity and lifespan based on performance goals. Based on experimental data from batteries used in electric vehicles, the battery pack was scaled down and developed using a 26.4 Ah capacity with a 2-RC circuit, as shown below [29].

$$V_{BT} = V_{OC} - I \times \left\{ R_0 + R_1 \left( 1 - e^{(-t/\tau_1)} \right) + R_2 \left( 1 - e^{(-t/\tau_1)} \right) \right\} \quad (13)$$

### 2.3. DC–DC Converter

A DC–DC converter was applied to convert the voltage generated by the fuel cell and battery to the required operating voltage for the motor. The voltage generated by both the fuel cell and the battery is lower than the motor's operating voltage, so a boost converter was used to step up the voltage. Additionally, while the fuel cell only produces and supplies power, the battery undergoes both charging and discharging. Therefore, the fuel cell system uses a unidirectional converter, while the battery uses a bidirectional converter.

### 2.4. Thrust Motor

A multicopter flies using thrust generated by two or more rotors, and is classified based on the number of rotors applied. One type of multicopter, the quadcopter, flies using thrust generated by four rotors. In this study, a DC motor was used for the application. The motor operates at an input voltage of 400 V, and the rotational speed varies according to the input current, which in turn determines the thrust. The motor used in this study is the Super-E S150 KV9.5, made in Nanchang, China and its specifications can be found in Table 2.

**Table 2.** Super-E S150 KV9.5 specification.

Current [A]	Speed [rpm]	Power [kW]	Thrust Force [N]
6.94	1166	2.33	250.84
12.46	1424	4.37	381.61
20.49	1684	7.38	538.67
33.39	1936	12.25	762.92
50.47	2197	18.56	1008.57
74.87	2449	27.27	1299.34
108.3	2703	38.64	1632.48

## 3. Results

### 3.1. Flight Profile

To evaluate the fuel cell–battery multicopter system, Figure 4 was applied based on the K-UAM (Korean Urban Air Mobility) operational concept document published by the Ministry of Land, Infrastructure, and Transport of Korea. The flight altitude is limited to 600 m, with the system configured to fly up to a maximum altitude of 500 m. The flight altitude profile was set with a Climb phase for altitude increase and a Descent phase for altitude decrease. Rapid altitude changes, such as steep climbs and descents, could reduce flight stability and cause discomfort for passengers [29]. Therefore, hovering flight was applied during altitude changes to ensure stability. It was confirmed that the system operates with the thrust generated by the four motors, maintaining appropriate altitude control and tracking the required altitude for climbing, descending, and hovering.

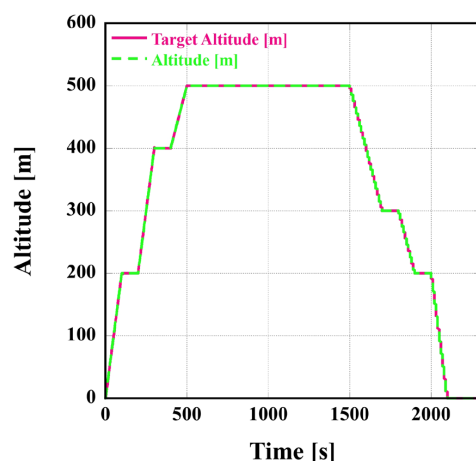


**Figure 4.** Hydrogen fuel cell–battery multicopter altitude cycle.

### 3.2. Power Management System

A hybrid system consisting of a hydrogen fuel cell system and a battery inherently requires strategies for power distribution based on load demand. The power management system optimizes power distribution between the fuel cell and the battery in response to real-time load variations, ensuring a stable power supply. Furthermore, efficient power distribution based on system states, such as load demand and battery SOC, can enhance the overall performance and efficiency of the system.

In this study, both Rule-Based and State Machine power management systems were applied, as shown in Figure 5 and Table 3. The power management system was configured for comparison based on a battery SOC of 45%, with subsequent power distribution determined by the system's load demand. In the Rule-Based power management system, the maximum power of the fuel cell was set to 138 kW, as specified by the manufacturer, while the normal power was set to correspond to the power at a load current density of 0.7 A/cm<sup>2</sup>. This range allows the fuel cell system to produce high-voltage power, as it represents a region where activation loss and resistive loss are balanced, and concentration loss is minimized. At lower current densities, hydrogen supply efficiency may decrease, whereas at higher current densities, insufficient flow rates can lead to system imbalances [30,31]. Therefore, the operating range of the fuel cell was configured to include both "max" and "normal" regions for power distribution. Additionally, during low SOC conditions, the fuel cell was operated at a power output higher than the load demand to recharge the battery.

The State Machine was implemented with 15 defined states based on battery SOC and load power. The battery SOC was categorized into three levels: Low, Medium, and High, with each level further divided into five detailed criteria for power distribution. When the load power is 30 kW, 60 kW, or 90 kW or less, the fuel cell power is set to the load power plus an additional 60 kW. If the load power is 120 kW or less, or exceeds 120 kW, the fuel cell takes full responsibility for the load power. For load powers of 30 kW, 60 kW, or 90 kW or less, the fuel cell power is configured to the load power plus 10 kW. If the load power is 120 kW or less, the fuel cell handles the load power minus 10 kW.

In cases where the load power exceeds 120 kW, the fuel cell power is set to the load power minus 25 kW. When the load power is 30 kW or 60 kW or less, the fuel cell assumes full responsibility for the load power. If the load power is 90 kW or less, the fuel cell handles the load power minus 20 kW. When the load power is 120 kW or less, the fuel cell manages the load power minus 25 kW. For load powers exceeding 120 kW, the fuel cell is configured to handle the load power minus 30 kW. This structured approach ensures efficient power distribution, adapting dynamically to the system's operational states and maintaining an optimal balance between the fuel cell and battery.

**Table 3.** State machine control states.

State	SOC [-]	Load Power [kW]	Fuel Cell Power [kW]
1	Low	$P_{load} > P_{Load,1}$	$P_{load} + P_{12}$
2	Low	$P_{load} > P_{Load,2}$	$P_{load} + P_{12}$
3	Low	$P_{load} > P_{Load,3}$	$P_{load} + P_{12}$
4	Low	$P_{load} > P_{Load,4}$	$P_{load}$
5	Low	$P_{load} > P_{Load,5}$	$P_{load}$
6	Medium	$P_{load} > P_{Load,1}$	$P_{load} + P_2$
7	Medium	$P_{load} > P_{Load,2}$	$P_{load} + P_4$
8	Medium	$P_{load} > P_{Load,3}$	$P_{load} + P_6$
9	Medium	$P_{load} > P_{Load,4}$	$P_{load}$
10	Medium	$P_{load} > P_{Load,5}$	$P_{load} - P_1$
11	High	$P_{load} > P_{Load,1}$	$P_{load}$
12	High	$P_{load} > P_{Load,2}$	$P_{load}$
13	High	$P_{load} > P_{Load,3}$	$P_{load} - P_4$
14	High	$P_{load} > P_{Load,4}$	$P_{load} - P_5$
15	High	$P_{load} > P_{Load,5}$	$P_{load} - P_6$

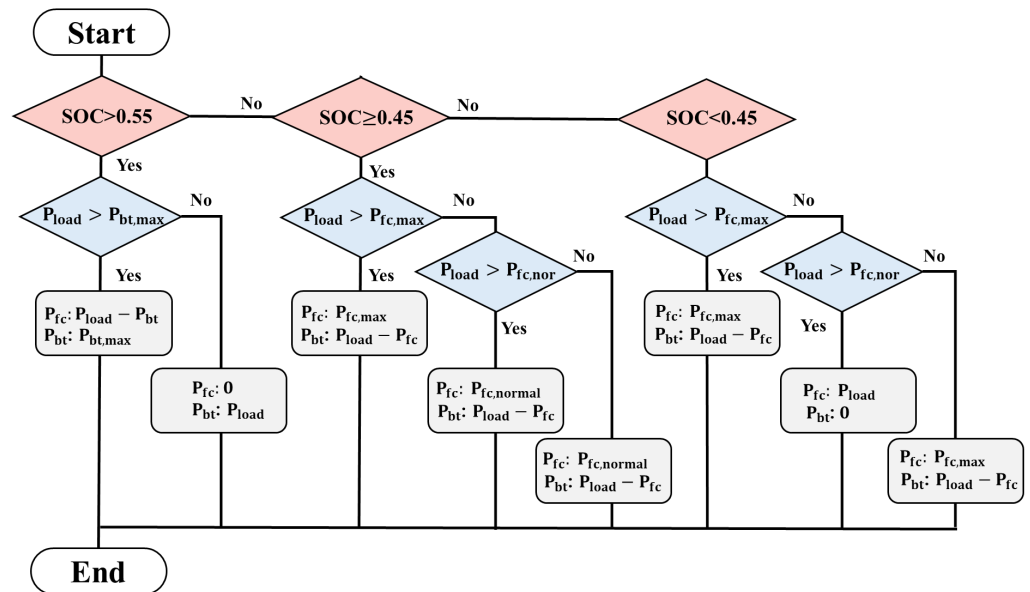


**Figure 5.** Flowchart of hydrogen fuel cell–battery hybrid multicopter power management system.

### 3.3. Multicopter System Performance

The power management system distributes the load power between the fuel cell and the battery based on the battery's state of charge (SOC) and load demand. A comparative analysis was conducted by applying the State Machine Control power management system and the Rule-Based power management system under an initial battery SOC of 45%. Figure 6 illustrates the load variations based on the power distribution strategies of the power management system under an initial SOC of 45%. Figure 6a shows the results of applying the Rule-Based power management system. Due to the low SOC, it can be observed that the fuel cell is primarily used during flight. Even after the flight ends and the aircraft lands at 2100 s, the fuel cell continues to charge the battery at normal power.

Figure 6b presents the graph for the State Machine power management system. Significant load variations occur as altitude changes, during which both the battery and the fuel cell are utilized. Additionally, after the flight ends at 2100 s, the fuel cell recharges the battery.

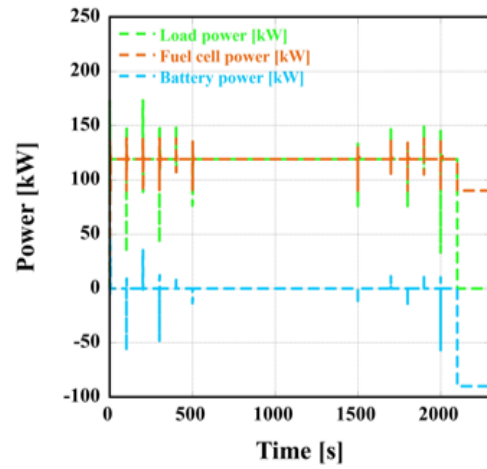
The variation in the power distribution strategies of the power management system also leads to changes in hydrogen consumption for operating the fuel cell system. The results of the calculated hydrogen consumption, as determined by the equation below [32], are shown in Figure 7. Both the State Machine and Rule-Based power management systems primarily rely on the fuel cell during flight. However, after landing, the Rule-Based system charges the battery more extensively, resulting in higher hydrogen consumption.

$$\dot{m}_{H_2} = \frac{I_{cell}}{2F} \quad (14)$$

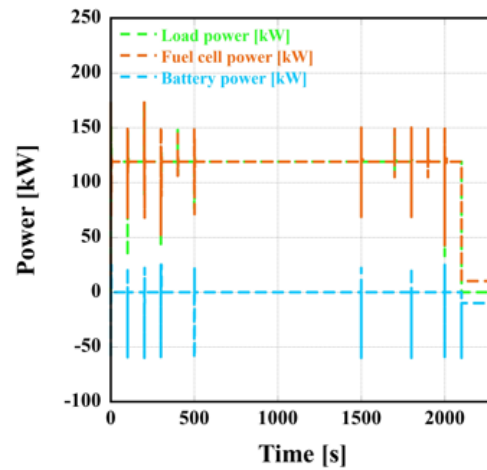
As a result, it was observed that hydrogen consumption in the State Machine system is approximately 5.85% lower compared to the Rule-Based system.

The battery SOC, influenced by the power distribution strategy of the power management system, is shown in Figure 8. Due to the low initial SOC, the fuel cell is primarily used during flight, resulting in the SOC remaining stable at 45% without significant decrease. After 2100 s, when the aircraft lands and the power demand drops to zero, the fuel cell begins recharging the battery. In the Rule-Based system, the fuel cell charges the battery at its normal power, whereas in the State Machine system, the fuel cell charges the battery

at 10 kW. This results in the SOC of the State Machine system being approximately 3.75% lower compared to the SOC of the Rule-Based system.



(a)



(b)

Figure 6. Power response with power management systems: (a) Rule-Based SOC 45%, (b) State Machine SOC 45%.

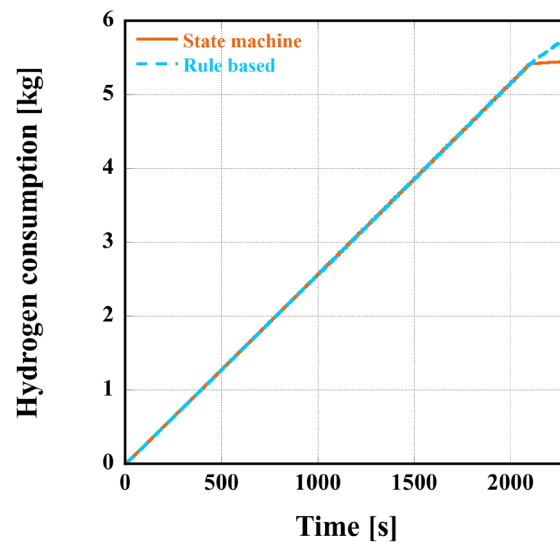
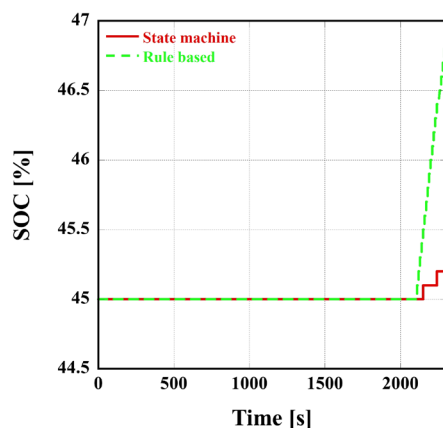


Figure 7. Comparison of hydrogen consumption in fuel cell system with initial SOC.



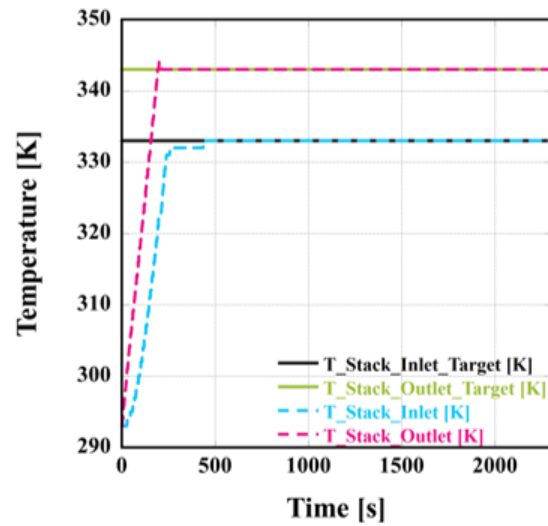
**Figure 8.** Change in SOC based on initial SOC.

As the load power of the fuel cell varies according to the power management system, an increase in load power results in higher heat generation, requiring thermal management system control to maintain optimal operating temperatures. Figure 9 shows the inlet and outlet temperatures of the fuel cell stack based on the power distribution strategies of the power management systems for the initial SOC. Figure 9a presents the inlet and outlet temperatures of the fuel cell stack with the Rule-Based system applied under an initial SOC of 45%. During flight, the fuel cell operates at high power, but the inlet temperature is maintained at the target temperature of 333.15 K through the control of the cooling fan. Similarly, the outlet temperature is maintained at 343.15 K by the cooling water pump. Despite variations in the required power due to altitude changes, the high-output operation of the fuel cell system ensures stable temperatures through the high flow rates of the cooling fan and pump, with minimal temperature fluctuations. Figure 9b illustrates the stack temperature results with the State Machine system applied under the same initial SOC of 45%. Similar to the Rule-Based system, the inlet and outlet temperatures are controlled at 333.15 K and 343.15 K, respectively, by the cooling fan and pump. However, after landing, the fuel cell output decreases significantly compared to the Rule-Based system, resulting in a noticeable reduction in the stack outlet temperature.

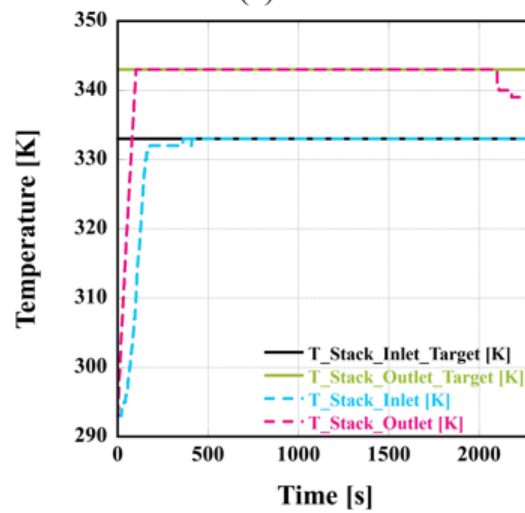
Lastly, for efficient thermal management of the fuel cell system, the cooling water pump and cooling fan are controlled to maintain the target temperature. However, the power consumed by the Balance of Plant (BOP) for temperature control and efficient operation of the fuel cell system is referred to as parasitic power, which reduces the overall system efficiency. The parasitic energy consumption of the hydrogen fuel cell–battery hybrid multicopter system during flight, based on the initial SOC, was calculated [33] as shown below and is illustrated in Figure 10.

$$\text{Pump}_{\text{Consumption}} = \int \text{Pump}_{\text{efficiency}} \times V \times I \quad (15)$$

$$\text{Fan}_{\text{Consumption}} = \int \text{Fan}_{\text{efficiency}} \times V \times I \quad (16)$$



(a)



(b)

Figure 9. Results of the temperature reaction of the fuel cell stack with power management system SOC: (a) Rule-Based SOC 45%, (b) State Machine SOC 45%.

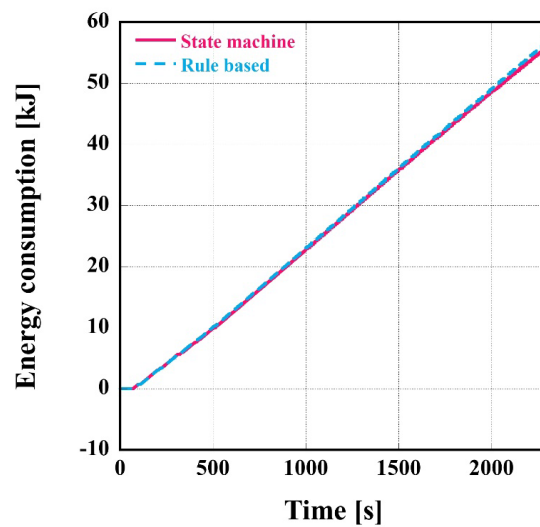


Figure 10. Parasitic energy consumption with initial SOC.

When the SOC is low, the use of the battery, which serves as an auxiliary power source, is limited, and the load power of the fuel cell increases. As a result, the heat generation of the fuel cell rises, leading to an increase in the required heat dissipation for temperature control, which in turn increases the required flow rate of the coolant pump and cooling fan. As a result, it can be observed that the State Machine achieves approximately a 1.63% reduction compared to the Rule-Based approach.

#### 4. Conclusions

In this study, a hydrogen fuel cell–battery hybrid multicopter system model was developed. The system behavior under an initial SOC of 45% was analyzed by applying State Machine and Rule-Based power management systems. The main findings are summarized as follows:

- (1) The multicopter system was configured with a 138 kW FC gen-HPS-based fuel cell system from Ballard and a 60 kW battery in a hybrid configuration for power supply.
- (2) Unidirectional and bidirectional DC–DC converters were applied to the fuel cell system and battery, respectively, to convert the power to the required operating voltage for the thrust motor, which was then used for flight.
- (3) Power distribution strategies for the hybrid fuel cell–battery system were implemented using State Machine and Rule-Based power management systems. The operation strategies based on battery SOC and load power were distributed within the defined operating range of the fuel cell system.
- (4) The hydrogen fuel cell–battery hybrid multicopter system was set to operate with an initial SOC of 45%, and the required power during flight was analyzed and compared by applying both the State Machine and Rule-Based power management systems.
- (5) At an initial SOC of 45%, the State Machine power management system resulted in a 5.85% reduction in hydrogen consumption and a 1.63% reduction in parasitic energy consumption compared to the Rule-Based power management system.

**Author Contributions:** J.C. developed and implemented the proposed hydrogen fuel cell–battery hybrid multicopter system design and power management optimization technique using AMESim. Literature reviews, formula analysis, and simulations were conducted by J.C. and H.-J.P. The review of system configurations, as well as the interpretation and verification of simulation results, were carried out by J.C. and H.-J.P. Final review of manuscript corrections was conducted by H.-J.P. and J.H. All authors have read and agreed to the published version of the manuscript.

**Funding:** This work was supported by the research grant of Kongju National University in 2023.

**Data Availability Statement:** Data are contained within the article.

**Acknowledgments:** This work was supported by the research grant of Kongju National University in 2023. The authors gratefully acknowledge this support from Kongju National University.

**Conflicts of Interest:** The authors declare no conflicts of interest.

#### Nomenclature

$A$	Active area [cm <sup>2</sup> ]
$E$	Open circuit voltage [V]
$F$	Faraday's constant [C/mol]
$g$	Gibbs free energy change [J/mol]
$\alpha$	Transfer coefficient [-]
$I$	Current [A]
$n$	Number of electrons [-]

$j_{stack}$	Stack current density [A/cm <sup>2</sup> ]
$j_0$	Exchange current density [A/cm <sup>2</sup> ]
$j_l$	Limiting current density [A/cm <sup>2</sup> ]
$\dot{m}$	Mol flow rate [mol/s]
$n$	Number of electrons [-]
$P$	Partial pressure [-]
$R$	Resistance [ $\Omega$ ]
$R$	Universal gas constant [J/K·mol]
$Stoi$	Stoichiometric ratio [-]
$T$	Temperature [K]
$V$	Voltage [V]
Subscripts and superscripts	
<i>Act</i>	Activation
<i>BT</i>	Battery
<i>Con</i>	Concentration
<i>conv</i>	Converter
<i>Ohm</i>	ohmic
Greek	
$\gamma$	Ratio of specific heat [-]
$\eta$	Efficiency [-]

## References

- Lim, J.; Choi, J.; Lee, J.; Choi, S. A Study on the Derivation of Safety Standards (Draft) for the Application of PEMFC Fuel Cells to Multicopters. In *2020 Korean Institute of Gas Conference Proceedings*; The Korean Institute of Gas: Seoul, Republic of Korea, 2020; p. 179.
- Arat, H.T.; Sürer, M.G. Experimental Investigation of Fuel Cell Usage on an Air Vehicle's Hybrid Propulsion System. *Int. J. Hydrogen Energy* **2020**, *45*, 26370–26378. [\[CrossRef\]](#)
- Garrow, L.A.; German, B.J.; Leonard, C.E. Urban Air Mobility: A Comprehensive Review and Comparative Analysis with Autonomous and Electric Ground Transportation for Informing Future Research. *Transp. Res. Part C Emerg. Technol.* **2021**, *132*, 103377. [\[CrossRef\]](#)
- Marzouk, O.A. Urban Air Mobility and Flying Cars: Overview, Examples, Prospects, Drawbacks, and Solutions. *Open Eng.* **2022**, *12*, 662–679. [\[CrossRef\]](#)
- Asmer, L.; Jaksche, R.; Pak, H.; Kokus, P. A city-centric approach to estimate and evaluate global Urban Air Mobility demand. *CEAS Aeronaut. J.* **2024**, 1–16. [\[CrossRef\]](#)
- Pinto Neto, E.C.; Baum, D.M.; De Almeida, J.R.; Camargo, J.B.; Cugnasca, P.S. A Trajectory Evaluation Platform for Urban Air Mobility (UAM). *IEEE Trans. Intell. Transp. Syst.* **2022**, *23*, 9136–9145. [\[CrossRef\]](#)
- Ferrare, F.D.; Moreira Baum, D.; De Almeida Junior, J.R.; Camargo Junior, J.B.; Cugnasca, P.S. Scenarios for the Use of eVTOLs Using Multiagent Systems With Netlogo: Comparison of Parameters and the Impact on UAM. In *Proceedings of the 2021 IEEE/AIAA 40th Digital Avionics Systems Conference (DASC)*, San Antonio, TX, USA, 3–7 October 2021; IEEE: San Antonio, TX, USA, 2021; pp. 1–7.
- Apeland, J.; Pavlou, D.; Hemmingsen, T. Suitability Analysis of Implementing a Fuel Cell on a Multirotor Drone. *J. Aerosp. Technol. Manag.* **2020**, *12*, e3220. [\[CrossRef\]](#)
- Corcau, J.-I.; Dinca, L.; Cican, G.; Ionescu, A.; Negru, M.; Bogateanu, R.; Cucu, A.-A. Studies Concerning Electrical Repowering of a Training Airplane Using Hydrogen Fuel Cells. *Aerospace* **2024**, *11*, 218. [\[CrossRef\]](#)
- Marinaro, G.; Di Lorenzo, G.; Pagano, A. From a Battery-Based to a PEM Fuel Cell-Based Propulsion Architecture on a Lightweight Full Electric Aircraft: A Comparative Numerical Study. *Aerospace* **2022**, *9*, 408. [\[CrossRef\]](#)
- An, J.-H.; Kwon, D.-Y.; Jeon, K.-S.; Tyan, M.; Lee, J.-W. Advanced Sizing Methodology for a Multi-Mode eVTOL UAV Powered by a Hydrogen Fuel Cell and Battery. *Aerospace* **2022**, *9*, 71. [\[CrossRef\]](#)
- Li, B.; Wan, K.; Xie, M.; Chu, T.; Wang, X.; Li, X.; Yang, D.; Ming, P.; Zhang, C. Durability degradation mechanism and consistency analysis for proton exchange membrane fuel cell stack. *Appl. Energy* **2022**, *314*, 119020. [\[CrossRef\]](#)
- Bahrami, M.; Martin, J.P.; Maranzana, G.; Pierfederici, S.; Weber, M.; Didierjean, S. Fuel cell management system: An approach to increase its durability. *Appl. Energy* **2022**, *306*, 118070. [\[CrossRef\]](#)
- Donateo, T. Simulation Approaches and Validation Issues for Open-Cathode Fuel Cell Systems in Manned and Unmanned Aerial Vehicles. *Energies* **2024**, *17*, 900. [\[CrossRef\]](#)

15. Baena Mejías, R.; Saias, C.A.; Roumeliotis, I.; Pachidis, V.; Bacic, M. Assessment of Hydrogen Gas Turbine-Fuel Cell Powerplant for Rotorcraft. *Int. J. Hydrogen Energy* **2024**, *50*, 772–783. [[CrossRef](#)]
16. Saib, S.; Achour, Y.; Ghennam, T.; Marouani, K.; Rizoug, N. Design Optimization and Power Management of a Fuel Cell-Battery Fixed-Wing Electric UAV. *Proc. Inst. Mech. Eng. Part G J. Aerosp. Eng.* **2024**, *238*, 76–88. [[CrossRef](#)]
17. Saib, S.; Hamouda, Z.; Marouani, K. Energy Management in a Fuel Cell Hybrid Electric Vehicle Using a Fuzzy Logic Approach. In Proceedings of the 2017 5th International Conference on Electrical Engineering—Boumerdes (ICEE-B), Boumerdes, Algeria, 29–31 October 2017; IEEE: Boumerdes, Algeria, 2017; pp. 1–4.
18. Li, H.; Sun, C.; Li, J.; Mei, J.; Jiang, J.; Fan, F.; Yang, W.; Zhuo, R.; Song, K. Self-Tuning Oxygen Excess Ratio Control for Proton Exchange Membrane Fuel Cells Under Dynamic Conditions. *Processes* **2024**, *12*, 2807. [[CrossRef](#)]
19. Lee, B.; Kwon, S.; Park, P.; Kim, K. Active Power Management System for an Unmanned Aerial Vehicle Powered by Solar Cells, a Fuel Cell, and Batteries. *IEEE Trans. Aerosp. Electron. Syst.* **2014**, *50*, 3167–3177. [[CrossRef](#)]
20. Erdör Türk, B.; Sarul, M.H.; Çengelci, E.; İyigün Karadağ, Ç.; Boyacı San, F.G.; Kılıç, M.; Okumuş, E.; Yazıcı, S. Integrated Process Control-Power Management System Design and Flight Performance Tests for Fuel Cell Powered Mini-Unmanned Aerial Vehicle. *Energy Technol.* **2021**, *9*, 2000879. [[CrossRef](#)]
21. Yang, Z.; Lei, T.; Lin, Z.; Fu, H.; Zhang, X. The Testing Platform of Hybrid Electric Power System for a Fuel Cell Unmanned Aerial Vehicle. In Proceedings of the 2018 IEEE International Conference on Electrical Systems for Aircraft, Railway, Ship Propulsion and Road Vehicles & International Transportation Electrification Conference (ESARS-ITEC), Nottingham, UK, 7–9 November 2018; IEEE: Nottingham, UK, 2018; pp. 1–8.
22. Lee, D.; Kim, B.; Lee, S. Load Fluctuation Mitigation and Stack Durability Experiments for Enhancing the Lifespan of Hydrogen Fuel Cell Electric Vehicles. *J. Korean Hydrogen New Energy Soc.* **2024**, *35*, 370–376. [[CrossRef](#)]
23. Song, J.-W. A Study on Two-Stage 700bar Hydrogen Regulator for FCEV. Master’s Thesis, Korea University of Technology and Education, Cheonan, Republic of Korea, 2020.
24. Kim, M.-S.; Kim, B.-J.; Byun, S.-Y.; Kim, D.-J.; Lee, S.-H. Study on the Steady-State and Dynamic Performance of Polymer Electrolyte Fuel Cells with Changes in External and Self-Humidification. *J. Korean Electrochem. Soc.* **2007**, *10*, 179–185. [[CrossRef](#)]
25. Zhang, G.; Kandlikar, S.G. A Critical Review of Cooling Techniques in Proton Exchange Membrane Fuel Cell Stacks. *Int. J. Hydrogen Energy* **2012**, *37*, 2412–2429. [[CrossRef](#)]
26. Sun, T.; Zhang, X.; Chen, B.; Liu, X. Coordination control strategy for the air management of heavy vehicle fuel cell engine. *Int. J. Hydrogen Energy* **2020**, *45*, 20360–20368. [[CrossRef](#)]
27. Chen, J.-H.; He, P.; Cai, S.-J.; He, Z.-H.; Zhu, H.-N.; Yu, Z.-Y.; Yang, L.-Z.; Tao, W.-Q. Modeling and Temperature Control of a Water-Cooled PEMFC System Using Intelligent Algorithms. *Appl. Energy* **2024**, *372*, 123790. [[CrossRef](#)]
28. Yu, S.; Jung, D. A Study of Operation Strategy of Cooling Module with Dynamic Fuel Cell System Model for Transportation Application. *Renew. Energy* **2010**, *35*, 2525–2532. [[CrossRef](#)]
29. Kim, S. An Empirical Study on Fear and Dizziness Using UAM Simulator. *J. Adv. Navig. Technol.* **2023**, *27*, 262–268.
30. Kim, M.-J. Design Technology Trends of Polymer Electrolyte Fuel Cells. *KIPE Mag.* **2007**, *12*, 25–28.
31. Srinivasan, S.; Velev, O.A.; Parthasarathy, A.; Manko, D.J.; Appleby, A.J. High Energy Efficiency and High Power Density Proton Exchange Membrane Fuel Cells—Electrode Kinetics and Mass Transport. *J. Power Sources* **1991**, *36*, 299–320. [[CrossRef](#)]
32. Kwon, D. Energy Consumption Rate Optimization of Hybrid eVTOL Propulsion Systems Using Hydrogen Fuel Cell Modeling. Master’s Thesis, Konkuk University, Seoul, Republic of Korea, 2023.
33. Yoo, S.; Kim, H.; Lee, S.; Lee, Y.; Ahn, K. Development of a Numerical Analysis Model for Thermal Management of Large-Area Polymer Electrolyte Fuel Cells. In Proceedings of the Korean Society of Mechanical Engineers Spring and Fall Conference, Busan, Republic of Korea, 30 May–1 June 2007; pp. 154–159.

**Disclaimer/Publisher’s Note:** The statements, opinions and data contained in all publications are solely those of the individual author(s) and contributor(s) and not of MDPI and/or the editor(s). MDPI and/or the editor(s) disclaim responsibility for any injury to people or property resulting from any ideas, methods, instructions or products referred to in the content.